2nd IFAC Workshop on Automatic Control in Offshore Oil and Gas Production,
May 27-29, 2015, Florianópolis, Brazil

A Methodology for Autonomous Robotic Manipulation of Valves Using Visual Sensing ⋆

Rafael O. Faria [*], **Florentin Kucharczak** [**]
Gustavo M. Freitas [*], **Antonio C. Leite** [*]
Fernando Lizarralde [*], **Mauricio Galassi** [***], **Pål J. From** [****]

[*] *Department of Electrical Engineering, COPPE*
Federal University of Rio de Janeiro, Rio de Janeiro, Brazil.
(e-mail: rafael.o.faria@gmail.com, fernando@coep.ufrj.br)

[**] *Department of Control, Vision and Robotics,*
Télécom Physique Strasbourg, Strasbourg, France.
(e-mail: flokucharczak@gmail.com)

[***] *Petrobras Research and Development Center,*
CENPES, Rio de Janeiro, Brazil.
(e-mail: mauricio.galassi@petrobras.com.br)

[****] *Department of Mathematical Sciences and Technology,*
Norwegian University of Life Science, Ås, Norway.
(e-mail: pal.johan.from@nmbu.no)

Abstract: This work presents a methodology for autonomous manipulation of valves using a dual-arm robot and the visual sensing provided by cameras mounted on the head and each robot arm. A novel image-based identification and pose estimation method is devised to determine the valve to be manipulated as well as to estimate its position and orientation with respect to the robot base. The valve pose is used in the positioning and alignment of the robot end effector enabling the manipulation task to be carried out autonomously. Experimental results, obtained with a Baxter^{TM} robot performing valve turning tasks, illustrate the feasibility of the proposed methodology. The main objective of this work is to provide capabilities to develop new solutions and innovative technologies to deal with the challenge of manipulating valves autonomously in poorly structured and harsh environments.

Keywords: Autonomous Operation, Dual-Arm Robot, Visual Estimation, Valve Manipulation.

1. INTRODUCTION

Offshore Oil & Gas industry is becoming increasingly dependent on efficient and low-cost solutions to justify the high investments associated with extracting oil in remote areas, in particular from wells with high exploration and operation costs. In addition, the oil companies consider the improvement of Health, Safety, and Environment (HSE) as a top priority in all their operations. Robotic solutions possess advantages for solving most of the abovementioned problems and are regarded a promising technology for making offshore platforms safer and more efficient. A natural consequence of these automated solutions is the reduction of human operators in unhealthy areas, which represents a significant improvement in HSE conditions on offshore platforms. In this context, robots can replace humans in tasks performed in unhealthy, hazardous, and confined areas. Several studies also point out the potential increase in efficiency and productivity with robot operators, as robots can work around the clock and perform a number of operations with higher accuracy and repeatability than humans (From, 2010). For example, Anisi et al. (2010) considers the use of robots in Oil & Gas facilities in operations that require both high precision and strength, regardless of weather conditions, using industrial robots.

Several research groups have developed mobile robots with different levels of autonomy for offshore automation. *Fraunhofer IPA* has for instance proposed a mobile robot for simple offshore inspection and maintenance tasks. One example is MIMROex (Bengel et al., 2009), which is capable of navigating safely in a cluttered environment, building maps, and executing inspection tasks autonomously. Another robot developed for offshore environments is Sensabot (NREC/CMU, 2012), capable of safely inspecting and monitoring hazardous and remote production facilities. The robot can sustain high temperatures, is able to reach areas with difficult access, and is certified to operate in explosive and toxic environments. SINTEF-ICT is another research group that is interested in applying robotic systems to the Oil & Gas industry, particularly

⋆ This work was partially supported by the Brazilian Funding Agencies CNPq, CAPES and the Norwegian Research Council.

in the topside of offshore platforms. Two industrial robot manipulators, mounted on a gantry crane and fixed on the floor, have been used to perform inspection and maintenance operations in a laboratory production process (Kyrkjebø et al., 2009). DORIS is an offshore inspection and monitoring robot being developed by COPPE/UFRJ in collaboration with Petrobras and Statoil. The robot moves on a rail carrying different sensors, analyzing sensor data *in loco* or storing it for future analysis. The sensors can identify abnormalities such as intruders in restricted areas, abandoned objects, smoke, fire, as well as liquid and gas leakages (Carvalho et al., 2013).

In the specific case of valve manipulation using robots, several studies have been developed since the early works (Trivedi et al., 1989; Abidi et al., 1991; Aspes et al., 1993). Underwater manipulation of valves is discussed in Palomeras et al. (2014), while Yoon et al. (2005) derive the motion process of the valve turning task from a teleoperation procedure. In Ahmadzadeh et al. (2013), a hierarchical autonomous valve-turning scheme for underwater robotics is developed and tested in a laboratory setup. An imitation learning approach is used to learn the reaching phase, while a hybrid force/motion controller is used for the turning phase (Ahmadzadeh et al., 2014).

Humanoid robots have also gained much attention in recent years and have been applied to valve operation. One of the tasks to be solved for the DARPA Robotics Challenge is to close three valves of different size and type using a humanoid robot (Alunni et al., 2014; Dellin et al., 2014; Hebert et al., 2014). Furthermore, Ajoudani et al. (2014) study the use of an intrinsically compliant humanoid robot for valve manipulation. The use of robot manipulators for offshore automation is still in its infancy and most projects focus on monitoring the offshore facilities rather than performing active intervention on the platforms.

In this paper, we present a methodology that uses a dual-arm robot for active manipulation of control valves. The robotic system is able to identify what valves to operate in a cluttered environment, estimate the pose of the selected valve and turn its wheel. Our approach only requires the user to remotely choose the target valve being able to operate it autonomously. We consider this work as our first step towards developing a complex autonomous robotic system for offshore automation.

2. PROBLEM FORMULATION

Consider the problem of autonomous robot-based manipulation of valves disposed with uncertain positions and orientations. Consider further that common industrial valves are used, with markers attached in their wheels. We propose to use point-light markers (e.g., LEDs), since these present less sensitivity to ambient light variations compared to ordinary markers. Although our methodology could also use other types of markers such as infrared or RFID (radio frequency identification) tags, which would require additional equipment, the purpose of this work is to focus on using the robot embedded sensors.

The markers are used to determine what valve has to be operated, named the *target valve*, and to estimate the location and orientation of the valves in the robot workspace. Here, the following assumptions are adopted: (A1) only one set of markers corresponding to the same valve is alight; (A2) there is no valve positioned in front of the other. In addition, we consider that the robot has neither prior knowledge of the valves pose, nor what valve should be operated. All decision-making and control are computed in real time based on the images captured by the cameras.

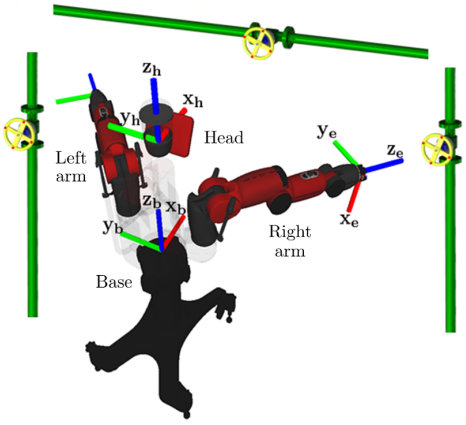

Fig. 1. Dual-arm robot and the valve system.

The robotic system discussed in this paper is a dual-arm robot equipped with a head camera in addition to eye-in-hand cameras on each manipulator. The head camera captures the whole workspace, which it uses to detect a set of LEDs identifying the target valve and estimating its position and orientation. The robotic system then chooses which robot arm to use for the operation, and approaches the selected arm to the valve. We use the camera attached to the wrist to position the end effector near the valve and to plan the manipulation task. Finally, the robot rotates the target valve and returns to the initial state waiting for a new target valve to manipulate. Fig. 1 shows the Baxter^{TM} robot, the coordinate systems and the valves in order to illustrate the problem formulation.

3. IMAGE-BASED POSE ESTIMATION SYSTEM

In this section, we present the image processing and pose estimation algorithms that integrate the image-based identification and pose estimation system. These algorithms will be used to (i) determine which valve has to be manipulated and to (ii) determine the position and orientation of the valve, estimating the normal vector of the plane formed by the attached LEDs.

3.1 Image Processing Algorithm

An important part of every visual-based identification and estimation system is the precise and efficient determination of the image features. According to Gao et al. (2003), at least three image features can be used to solve the Perspective-n-Point (PnP) problem. In our work, for the sake of simplicity we use four common LEDs as visual markers attached to the valve wheel (see Fig. 2). Indeed, considering four point-light markers the PnP problem becomes less complex to solve due to the redundancy of visual information (Oberkampf et al., 1996).

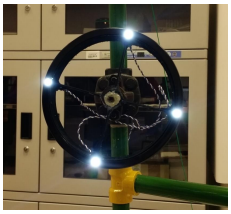

Fig. 2. Valve prototype and the attached LEDs.

Several techniques for the detection of light sources can be found in literature (Bouganis and Brookes, 2004; Lopez-Moreno et al., 2013). However, for the case of bright blob detection, the proposed methodologies are based on relative detection of the maximum brightness. In fact, the tracked features are determined in function of the maximum value of the image brightness. This assumption can not be considered for LEDs detection since the image-based algorithm must be robust to the existence of any other light sources, considering reflections as well. The great advantage of this methodology is the possibility of obtaining a really reliable binary output in the presence (or not) of the four markers in the current image frame, regardless of the scenario. The methodology developed to perform the LEDs detection is composed of four main steps, described in the following:

Step 1 - CIE LUV conversion: After setting the intrinsic parameters of the camera, each image frame recorded is converted from the traditional RGB color space to the CIE LUV color space (Trezona, 2001) as seen in Fig. 3(a). The key idea is to extract the LEDs features from the image background. It is worth mentioning that among the color representations tested, each one with different purposes, CIE LUV presents the best performance in terms of features dissociation. Indeed, the great benefit of this color space conversion is an increase of the background attenuation and edge enhancement ratio for the LEDs;

Step 2 - Selection of Lightness Channel: The third channel of the LUV image is a gray scale representation of the gamma-corrected brightness component of the color. In this step, we create a new image, as seen in Fig. 3(b), using only the "V" channel as our main interest is to keep, extract and enhance the LEDs edges;

Step 3 - Canny Filtering: From Fig. 3(b), we can see that the variations in the light halo are much more important than the light itself. In this step, the objective is to remove all visual information from the image that does not belong to the LEDs contour, using the well-known Canny filter (Canny, 1986). This image processing filter is composed of different steps as well. The first one is the application of a 2D Gaussian filter in order to attenuate noise. The second step aims to find the intensity gradient of the image, applying a pair of vertical and horizontal gradient convolution masks. Then, the intensity and direction of the 2D gradient is calculated. The last step consists in determining whether a pixel belongs to the contour, performing a non-maximum suppression and hysteresis thresholding method. The lower and upper values of the gray scale thresholds are chosen as $\mu_1 = 100\ pixel$ and $\mu_2 = 200\ pixel$ respectively, in order to obtain a robust contour detection;

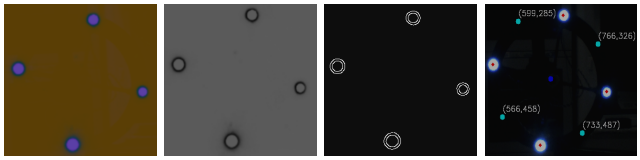

(a) (b) (c) (d)

Fig. 3. The steps of LEDs detection methodology: (a) CIE LUV conversion; (b) V channel selection; (c) Canny filtering; (d) Contour selection.

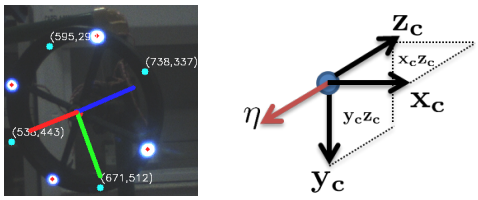

(a) (b)

Fig. 4. Normal vector representation of the valve wheel: (a) Image frame $\mathcal{F}_v$; (b) Camera frame $\mathcal{F}_c$.

Step 4 - Contour Selection: In order to find the centroid coordinates for each LED in the image, a range of feasible radius and minimum values for the solidity condition were defined. The solidity condition is defined as the ratio of contour area to its convex hull area, where a value close to unity implies in a circular edge. However, in general, the detection algorithm finds more than one contour representing the same LED which generates a number of candidate centroid coordinates. To overcome this multiple solutions problem, we propose to calculate the mean value of the coordinates for all centroids of the same LED in order to determine only one centroid for each.

Since the valves are fixed on the panels with different poses, it is necessary to obtain some extra information about the relative pose between the robot end effector and the lighted valve. The Baxter robot is equipped with a monocular video camera in both hands, and, thus, the visual-based estimation problem consists in using the relationship between 3D points of the real scenario and its 2D projections in the image frame $\mathcal{F}_v$ to calculate the valve pose in the camera frame $\mathcal{F}_c$ (PnP problem). In the presented solution, an iterative pose estimation is performed using coplanar feature points (Oberkampf et al., 1996) represented by the valve markers. Then, from the corners coordinates of the square formed by the LEDs and their correspondent 2D projections in the image frame $\mathcal{F}_v$, it is possible to estimate the valve pose (Fig. 4).

3.2 Pose Estimation Algorithm

In this section, we present the pose estimation algorithm used to calculate the normal vector to the plane formed by the LEDs, in order to obtain the valve pose. The pose estimation algorithm provides the distance from the camera center to the object center in the image plane, as well as the normal vector $\boldsymbol{\eta}$, which indicates the direction where the valve plane is pointing to, with respect to the camera frame $\mathcal{F}_c$, as shown in Fig. 4. The normal vector also indicates the final direction which the robot end effector should be pointing to, and it will be used to

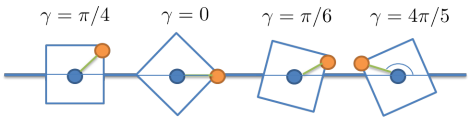

Fig. 5. Calculation of the roll angle for the end effector.

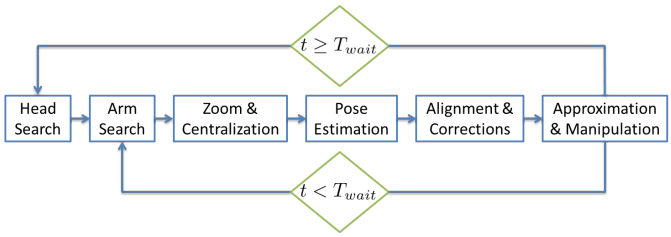

Fig. 6. Six-step sequence of operation.

generate the desired orientation for the robot end effector. Let α be the *pitch* angle, that is, the angle between the normal vector $\boldsymbol{\eta}$ and the horizontal plane (x_c-z_c). In addition, let β be the *yaw* angle, that is, the angle between the normal vector $\boldsymbol{\eta}$ and the vertical plane (y_c-z_c).

The angle α can be obtained from the inner product between the unitary vectors $\boldsymbol{\eta}_{yz}$ and $\boldsymbol{y}_c$ as:

$$\alpha = \arccos(\boldsymbol{\eta}_{yz} \cdot \boldsymbol{y}_c) - \pi/2\,, \tag{1}$$

where $\boldsymbol{\eta}_{yz}$ is the projection of vector η into vertical plane (y_c-z_c). Similarly, the angle β can be obtained from the inner product between the unitary vectors $\boldsymbol{\eta}_{xz}$ and $\boldsymbol{x}_c$ as:

$$\beta = \arccos(\boldsymbol{\eta}_{xz} \cdot \boldsymbol{x}_c) - \pi/2\,, \tag{2}$$

where $\boldsymbol{\eta}_{xz}$ is the projection of vector $\boldsymbol{\eta}$ into the horizontal plane (x_c-z_c). The roll angle ϕ is defined as the angle which the robot end effector has to turn in order to position the gripper inside the valve wheel so that it is far from the valves spokes or bars. From Fig. 5, we define γ as the angle between the horizontal line and the LED closest to this line. Then, it is possible to compute the angle ϕ as:

$$\phi = \begin{cases} \pi/4 - \gamma\,, & \gamma \leq \pi/2\,, \\ \pi - (\pi/4 + \gamma)\,, & \gamma > \pi/2\,. \end{cases} \tag{3}$$

It is worth mentioning that it is enough to rotate only the last joint of the arm by the angle γ to avoid the collision with the valve spokes.

4. OPERATING PROCEDURE

In this section, we develop a sequence of operations, using the modular functionality of each step as a guideline (Fig. 6). It is assumed that the robot does not know which valve it has to operate. So, the first step in the algorithm is to use the head camera to search if there is any valve lighted up and, if so, obtain the approximate position of it (*Head Search* step).

The search starts moving the head camera by an angle θ on a range from π to $-\pi$ (Fig. 7). From Fig. 8, the two blue stripes mark the region of interest $\mathcal{R}$, defined near the centre of the image, and the four red dots indicate the position of the detected LEDs. If four LEDs are detected and they are within the region $\mathcal{R}$, the robot stops searching at that point and saves the angle θ. In case the head reaches the angle π without detecting any LEDs, the search continues while it returns to the initial position.

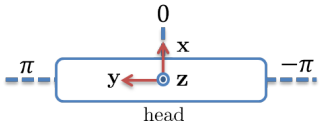

Fig. 7. Coordinate system of the robot head.

Fig. 8. Head camera view during the *Head Search* step.

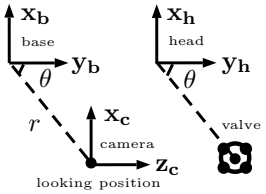

Fig. 9. Alignment between the camera and robot frames.

This step will continue until the operator finally turns on the LEDs and the robot detects it.

Now, depending on the value of angle θ, the robotic system will place one of the arms in a suitable position (looking position), so that the hand camera can visualize the panel which has the lighted up valve (*Arm Search* step). The looking position p_l depends on the angle θ and can be defined as $p_l = [\, r\sin(\theta) \quad r\cos(\theta) \quad z_l \,]^\intercal$, where $r \in \mathbb{R}$ is the actuation radius (see Fig. 9) and $z_l \in \mathbb{R}$ is defined ad-hoc. If $\theta \geq 0$ the left arm is chosen; otherwise, if $\theta < 0$ the right arm is selected. From that point, we can activate the hand camera of the selected arm and use the image-based algorithm from Section 3. We choose to keep the camera always aligned with the y_r-z_r plane, so that the visual estimation of the normal vector can be simplified (Fig. 9). Note that, the camera is kept aligned with the robot y_b-z_b plane and this assumption avoids image distortions during the visual estimation. The algorithm will return the orientation of the valve as well as the distance between the valve center and the camera center, with respect to the camera frame $\mathcal{F}_c$.

According to our experiments, in order to obtain a better visual estimation it is recommended to approximate the camera to the valve and centralize them, before doing the final estimation (*Zoom & Centralization* step). So, we use the first estimation to position the arm close enough to the valve, keeping a certain distance $d \in \mathbb{R}$, which is neither too close nor too far away from it. We also found out that the estimation of the coordinate z_c is precise enough, but the estimation of coordinates x_c and y_c are not. So, in order to minimize the positioning errors, we proposed to centralize the valve and the images centers. The alignment is performed using the kinematic control scheme described

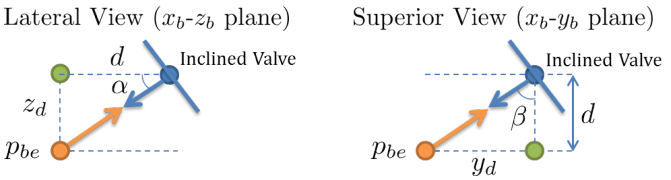

Fig. 10. Correction of end-effector position.

in the Section 5.2. We use the rotation matrix, denoted by $R_{bc} \in SO(3)$[1], to transform the coordinates of the error vector in the camera frame $\mathcal{F}_c$ into the coordinates of the same vector in the base frame $\mathcal{F}_b$ according to the composition of rotation matrices given by $R_{bc} = R_{be}\, R_{ec}$ where $R_{ec} = R_z(-\pi/2)$ is the rotation matrix of the camera frame $\mathcal{F}_c$ with respect to the end-effector frame $\mathcal{F}_e$, and R_{be} is the rotation matrix of the end-effector frame $\mathcal{F}_e$ with respect to the robot base frame $\mathcal{F}_b$, to be defined.

Once the hand camera is closer and aligned, the pose of the valve is estimated again in order to obtain a more precise result (*Pose Estimation* step). The estimation needs to be precise, since it will be used to determine the relative pose between the end effector and the valve. So, we implemented a digital filter to the estimated output data, that is, roll, pitch and yaw angles and the position vector. The filter first eliminates eventually undesired measures, such as, the values of pitch and yaw angles greater in module than 1.3 *rad*. Then, the filter takes the mean of all estimated values and it also eliminates estimations that are two standard deviation above this mean.

Using the filtered estimation, the arm is placed in front of the valve and the end effector is aligned at the normal direction to the valve plane. However, since any change in the end-effector orientation will result in misalignment with respect to the valve center, it is necessary to calculate the updated position of the end effector by the following correction equations:

$$z_d = d\, \tan(\alpha)\,, \qquad y_d = d\, \tan(\beta)\,, \tag{4}$$

where $z_d \in \mathbb{R}$ is the height that the end effector should go down/up and $y_d \in \mathbb{R}$ is the lateral distance that the end effector should go left/right in order to be normal to the valve plane (Fig. 10).

Another important concern is that we obtained the measures with respect to the camera frame $\mathcal{F}_c$, but the end-effector center is located in a different point. So, we first correct this *offset* and use the z_d and y_d values from the correction equations. Let $p_0 \in \mathbb{R}^3$ be the robot position which is zoomed and centralized to the valve. The final pose of the robot end effector is given by:

$$p_{be} = p_0 + [\ 0 \quad d_y + y_d \quad d_z + z_d\ ]^{\mathsf{T}}\,, \tag{5}$$

$$R_{be} = R_y(\pi/2)\ R_x(\beta)\ R_y(\alpha)\ R_z(\phi)\,, \tag{6}$$

where $p_{be} \in \mathbb{R}^3$ and $R_{be} \in SO(3)$ denote the position and orientation of the end effector with respect to the robot base; R_x, R_y and R_z are elementary rotation matrices around x, y, and z axes, respectively; $d_y = 0.034\ m$ and $d_z = -0.026\ m$ are the *offset* between the camera and the end-effector frames. The above equations comprise the *Alignment & Corrections* step.

Finally, we use the kinematic control scheme to move the end effector to the desired pose and, after that, we define a straight line as the new reference which the robot arm has to follow (*Approximation & Manipulation* step). The distance to travel is defined as $d_t = \sqrt{z_d^2 + y_d^2}$ minus a small security value, to ensure that the end effector will not touch the valve. Once this movement is finished, the gripper is inside the valve and the robotic system only rotates the last joint of the arm to perform the manipulation. After that, the robot arm follows the same straight line in the opposite direction. To conclude the manipulation task, the arm returns to the Looking position.

It is still necessary to determine what to do after the first manipulation. In order to increase the autonomy of the robotic system, we decided to wait a period of time T_{wait} for the last activated camera continues to look for some valve at the same panel. If during this period a valve of this panel is lighted up, the algorithm jumps to *Arm Search* step. However, if the time T_{wait} is over, the *Head Search* step is activated again and the head camera starts to find any lightened valve, as already described.

In the case of occlusion of one or more LEDs, the visual estimation algorithm continues in the *Arm Search* step until finding the adequate number of visual markers. If the detection is not succeeded during a given period of time, the current step stops and the algorithm returns to the *Head Search* operation.

5. EXPERIMENTAL SETUP AND RESULTS

In this section, we present the experimental evaluation of the proposed methodology[2]. We first briefly describe the equipment and the experimental setup used to perform the tests of autonomous valve manipulation. Next, we present practical results to illustrate the feasibility of our proposal.

5.1 Experimental setup

The robotic system is composed by a Baxter™ Robot (Rethink Robotics) with 7-DoF per arm for maximum flexibility and range, where each arm is endowed by an interchangeable end effector and a video camera for recognizing objects, parts and workspace (Guizzo and Ackerman, 2012). Baxter also has a 360 degrees sonar array and a front camera mounted in its head for human presence detection. Each arm has torque, velocity and position sensing in each joint. Other integrated sensors are 3-axis accelerometers and infrared range finders in each wrist, however these were not used to perform the valve manipulation task.

In the experiments, we have used a Baxter Research Robot. The main difference compared to the industrial model is related to the software. The research model is able to perform tasks according to the algorithms developed with the open-source Robot Operating System (ROS) platform (Quigley et al., 2009). Based on the manufacturer Unified Robot Description Format (URDF) model, we have created a simplified representation of the robot arm

[1] The term $SO(3)$ denotes the special orthogonal group or the rotation group for the three-dimensional space.

[2] The experiments can be viewed in the accompanying video clip in: https://www.youtube.com/embed/szRbhB58YMY?rel=0

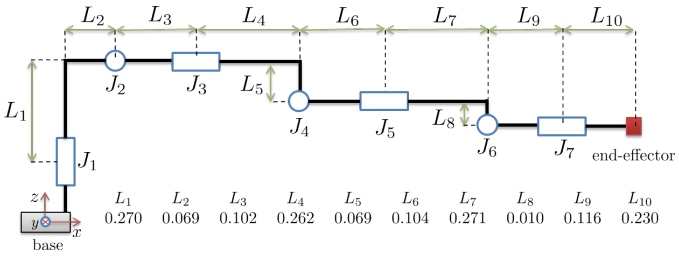

Fig. 11. Links and joints representation for the Baxter arm.

(Fig. 11), where the links lengths L_i are expressed in meters and the robot joints J_i are of revolution type. From this model, we can obtain the standard parameters of the Denavit-Hartenberg convention for the robot arm (Siciliano et al., 2010).

The operating environment has two task panels, each one supporting a set of four valves *ad hoc* adapted with four attached LEDs to carry out proof-of-concept experiments. The valves are located in the robot workspace and installed in different positions and orientations, requiring different capabilities from the robotic system. In order to simplify the manipulation task, the valves have been modified. Due to the torque limitations of the Baxter joints, the wheels are not rigidly connected to the valves stems, being able to rotate freely. Another adaptation was to couple four LEDs in each wheel, which helps the robot to identify the target valve and estimates its position and orientation.

The precision of the valve manipulation task depends on the robot positional accuracy, which is about 5 mm for the whole workspace, according to the manufacturer. In order to succeed in the experiments, the 12 mm thick end-effector fingers have to go inside the valve wheel (55 mm of radius). If we consider the end effector correctly aligned to the valve centre, the maximum acceptable positioning error due to visual estimation inaccuracy is about half of the valve radius, that is, 27.5 mm.

As previously mentioned, there are three cameras available locally on the robot. A single camera is located in either of Baxter's hands, on the left and right, and a third camera is positioned on Baxter's head. In the experiments, the head camera was used to locate the valve highlighted by the LEDs, whereas the cameras mounted in the eye-in-hand configuration were used to identify the normal vector to the plane formed by the LEDs, during the alignment, positioning, and approaching phases.

Due to limited bandwidth capabilities of the Baxter visual system only two cameras can be used simultaneously and it is not straightforward to interchange among the three built-in cameras in real time. Thus, for the experiments, we selected the two hand cameras and replaced the head camera by a Logitech HD Webcam C270, directly connected to the computer by a USB port. Default behavior on Baxter startup is for both of the hand cameras operate at a resolution of 320×200 $pixels$ at a frame rate of 25 fps. In the experiments, we used the resolution of 1280×800 $pixels$ at a frame rate of 20 fps for all cameras. Finally, before running the image processing routine, we have to determine the image distortion coefficients (radial and tangential) k, as well as the focal length f, the principal point coordinates c_x, c_y and the skew coefficient α_s, using a conventional calibration method provided by the OpenCV library. The calibrated camera parameters are: $f\alpha_s = 402.3$ $pixel$, $c_x = 669.6$ $pixel$, $c_y = 404.3$ $pixel$.

5.2 Robotic manipulator control

In this section, we consider the pose regulation problem for the Baxter robot. A control scheme based on the inverse kinematics algorithm with Jacobian pseudo-inverse is used. Let $p_d \in \mathbb{R}^3$ and $R_{bd} \in SO(3)$ be the desired (constant) position and orientation. Let $p \in \mathbb{R}^3$ and $R \in SO(3)$ be the current end-effector position and orientation. The arm pose is obtained from the forward kinematics map expressed in terms of the manipulator joint angles $q \in \mathbb{R}^n$.

We adopt a non-singular representation for the current orientation R_{be} and the desired orientation R_{bd} given by the correspondent unit quaternions $\mathcal{Q} = [\,\mathcal{Q}_s \;\; \mathcal{Q}_v^\mathsf{T}\,]^\mathsf{T} \in \mathbb{H}$ and $\mathcal{Q}_d = [\,\mathcal{Q}_{sd} \;\; \mathcal{Q}_{vd}^\mathsf{T}\,]^\mathsf{T} \in \mathbb{H}$, respectively. Notice that, $\mathcal{Q}_s, \mathcal{Q}_{sd} \in \mathbb{R}$ are the scalar parts and $\mathcal{Q}_v, \mathcal{Q}_{vd} \in \mathbb{R}^3$ are the vector parts of the quaternions[3]. The position and orientation errors of the end effector, given by $e_p \in \mathbb{R}^3$ and $e_o \in \mathbb{R}^3$, can be computed using the following equations (Siciliano et al., 2010):

$$e_p = p_d - p\,, \tag{7}$$

$$e_o = \Delta\mathcal{Q}_v = \mathcal{Q}_s\,\mathcal{Q}_{vd} - \mathcal{Q}_{sd}\,\mathcal{Q}_v - S(\mathcal{Q}_{vd})\,\mathcal{Q}_v\,, \tag{8}$$

where S is the skew symmetric operator and e_o is the vector component of the quaternion error.

The control objective is defined as:

$$p \to p_d \quad \therefore\; e_p = [\,0\;\,0\;\,0\,]^\mathsf{T}\,, \tag{9}$$

$$\mathcal{Q}_v \to \mathcal{Q}_{vd} \quad \therefore\; e_o = [\,0\;\,0\;\,0\,]^\mathsf{T}\,. \tag{10}$$

A control law $u \in \mathbb{R}^n$ which drives the pose error $e \in \mathbb{R}^6$ asymptotically to zero is given by:

$$u = J^* \underbrace{\begin{bmatrix} K_p & 0 \\ 0 & K_o \end{bmatrix}}_{K} \underbrace{\begin{bmatrix} e_p \\ e_o \end{bmatrix}}_{e}\,, \tag{11}$$

where the position and orientation gain matrices are given by $K_p = k_p\, I_3$ and $K_o = k_o\, I_3$ respectively, where k_p and k_o are scalar gains. To overcome the singularities problem in the Jacobian matrix J, a *damped least-squares (DLS)* pseudo inverse is used:

$$J^* = J^\mathsf{T}\,\left(\,J\,J^\mathsf{T} + \lambda^2\, I_6\,\right)^{-1}\,, \tag{12}$$

where $\lambda \in \mathbb{R}$ is the damping factor which is properly chosen, since a fixed value for λ could prevent the end effector to reach the desired pose. The scalar λ can be defined in terms of the manipulability measure $w(q) = \sqrt{\det\,(J\,J^\mathsf{T})}$ as $\lambda = \|e\|/w(q)$.

Since the Baxter arm is redundant, we can exploit the redundance of the Jacobian using optimal control to minimize a functional (Siciliano et al., 2010). The Baxter arm has tight joint limits, thus we can use the arm redundancy considering a secondary objective functional:

$$\mu = -\left(\frac{1}{n}\right)\sum_{1}^{n}\frac{(q_i - \bar{q}_i)}{(q_{iM} - q_{im})^2}\,, \tag{13}$$

where q_i is the current i-th joint angle, q_{iM} is the maximum limit of the i-th joint angle, q_{im} is the minimum limit

[3] The symbol $\mathbb{H}$ denotes the unit quaternion group satisfying the algebra of quaternion (Siciliano et al., 2010).

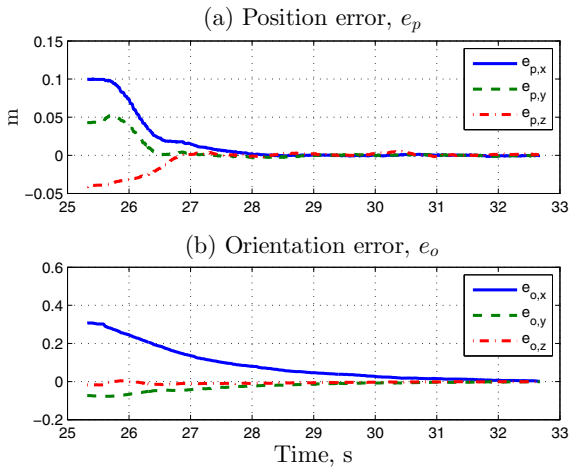

Fig. 12. Errors signals: (a) position e_p; (b) orientation e_o.

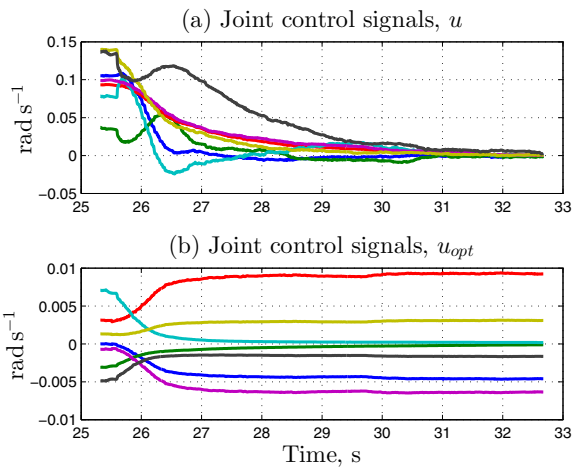

Fig. 13. Joint control signals: (a) u; (b) u_{opt}.

and $\bar{q}_i$ is the middle value of i-th joint range. The second component of the control law, denoted by u_{opt}, is given by:

$$u_{opt} = (I_7 - J^* J)\, k_j\, \mu\,, \tag{14}$$

where k_j is a constant gain. Thus, based on the kinematic control approach, the joint velocity control signal $\dot{q} \in \mathbb{R}^n$ can be obtained as:

$$\dot{q} = u + u_{opt} = J^*\, K\, e + (I_7 - J^* J)\, k_j\, \mu\,, \tag{15}$$

where $K = diag\{K_p, K_o\}$ is the pose gain matrix.

5.3 Practical results

In the experimental tests, the Baxter robot has to visually identify the valve of interest, lighted by the LEDs, and turn the valve wheel clockwise or counter-clockwise, according to the priority sequence assigned by the operator. As described in the Operating Procedure section, the valve manipulation task is composed of 6 steps (Fig. 6).

We collected data during the experiment under the kinematic control focusing on the alignment and correction step, since this phase requires the continuous change of both position and orientation of the robot end effector. The control algorithm is implemented in Python and the control loop of the program runs on a computer at sampling time of 20 ms on a 3.4 GHz Intel i7-3770 processor with 4 Gb RAM. We connect the PC to Baxter over LAN using a Linux workstation running ROS and the Baxter SDK, an Open-source Software Development Kit. The control parameters were: $k_p = 0.8\ s^{-1}$, $k_o = 0.7\ rad\, s^{-1}$, and $k_j = 20$.

Fig. 12(a) and (b) illustrate the position and orientation errors of the robot end effector, denoted respectively by e_p and e_o, during the experiment. The time history of the joint control signals u and u_{opt} is presented in Fig. 13(a) and (b) respectively. As can be observed, the position and orientation errors convergence asymptotically to zero, and the joint velocity control signals vanish.

It is worth mentioning that exhaustive experiments were conducted to demonstrate the performance of the pose control scheme for the robot end effector. To evaluate the performance of the visual estimation algorithm 20 additional tests were carried out, where the Baxter robot had to manipulate the valves located at different positions

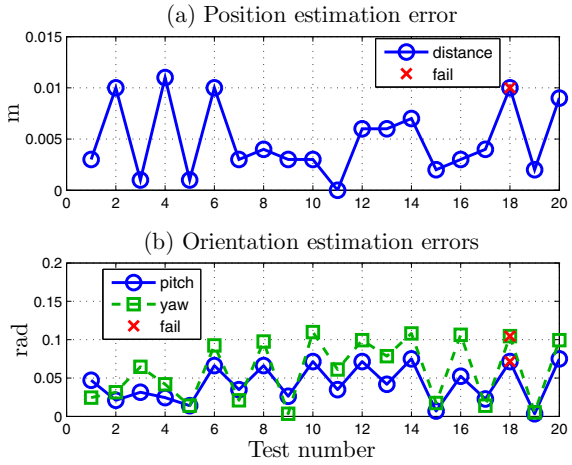

Fig. 14. Estimation errors: (a) valve position; (b) valve orientation.

and orientations. The estimation errors are presented in Fig. 14(a) and (b), where it is possible to observe the small magnitude of the valve position and orientation errors. Satisfactory results were achieved and about 95% of the test were properly performed. The manipulation has failed at Test 18 due to the combination of high values of the pitch, yaw and distance errors. The main reason of this erroneous manipulation comes from the imprecise spacing of the LEDs located at the valve wheels. Thus, the improvement of the robustness and accuracy of the visual estimation algorithm, with respect to positioning uncertainties of the point-light markers, could leverage the experimental results.

6. CONCLUDING REMARKS AND PERSPECTIVES

In this paper, we present a methodology for autonomous manipulation of control valves by using a dual-arm robot and the visual information provided by two video cameras mounted in each arm in the eye-in-hand configuration. The control scheme for positioning the robot end effector and regulation of its orientation is based on the inverse kinematics algorithm, which uses the pseudo-inverse of the Jacobian matrix and an additional term of projection

to avoid the mechanical joint limits. The visual detection system is designed in terms of an image-based identification and estimation algorithm, which visually identifies the valve to be manipulated looking for a set of lighted LEDs attached to the valve wheel and estimates the normal vector to the plane formed by the LEDs.

Experimental tests, performed with a Baxter™Robot and a simplified valves system developed ad-hoc for proof-of-concept purpose, were presented to illustrate the feasibility of the proposed scheme. Furthermore, it is noteworthy to mention that the proposed methodology could be extended for application in Oil & Gas production systems provided that the simplifying assumptions can be changed. First, we considered that all valves to be manipulated were located within the robot workspace, but in a real scenario the robot should be mounted on the top of a mobile vehicle or rail to increase its dexterity and reach. In the experimental tests we only consider valves with the same type of manual handwheel (mass and dimension), but the key idea is to develop a library of wheels based on the most common models of control valves available on an offshore plant. In this context, to manipulate any sort of control valves, with different sizes, we have to use a robot arm with higher torque capacity and force feedback.

Future works following the ideas developed here are: (i) implementing an obstacle avoidance and detection algorithm enabling the robot to operate in unstructured environments; (ii) considering the presence of uncertainty in the robot kinematic and dynamic parameters, which is a more realistic assumption from the practical point of view, particularly when the robot end effector grasps different objects to use as a tool; (iii) extending the proposed approach to consider different types and sizes of valves commonly found in refineries and Oil & Gas platforms; (iv) utilizing faster and more accurate image processing techniques to reduce the execution time of the LEDs detection algorithm; (v) developing new experiments with IR cameras and sensors to increase the robustness of the robotic system to image disturbances caused by the usual presence of smoke and steam in the working environment.

ACKNOWLEDGMENTS

The authors would like to thank Rodrigo D. Estrada and Thais B. Joffe for the construction of the valve panels, its electronics and the support during the experiments.

REFERENCES

Abidi, M., Eason, R., and Gonzalez, R.C. (1991). Autonomous robotic inspection and manipulation using multisensor feedback. *Computer*, 24(4), 17–31.

Ahmadzadeh, S.R., Jamisola, R.S., Kormushev, P., and Caldwell, D.G. (2014). Learning Reactive Robot Behavior for Autonomous Valve Turning. In *Proc. of IEEE-RAS Int. Conf. on Humanoid Robots*.

Ahmadzadeh, S.R., Kormushev, P., and Caldwell, D.G. (2013). Autonomous Robotic Valve Turning: A Hierarchical Learning Approach. In *Proc. of IEEE Int. Conf. on Robot. and Autom.*, 4614–4619.

Ajoudani, A., Lee, J., Rocchi, A., Ferrati, M., Hoffman, E.M., Settimi, A., Caldwell, D.G., Bicchi, A., and Tsagarakis, N.G. (2014). Manipulation Framework for Compliant Humanoid COMAN: Application to a Valve Turning Task. In *Proc. of IEEE-RAS Int. Conf. on Humanoid Robots*.

Alunni, N., Suay, H.B., Phillips-Grafflin, C., Mainprice, J., Berenson, D., Chernova, S., Lindeman, R.W., Lofaro, D.M., and Oh, P.Y. (2014). Towards a User-guided Manipulation Framework for High-DOF Robots with Limited Communication. *Intell. Service Robot.*, 7(3), 121–131.

Anisi, D.A., Gunnar, J., Lillehagen, T., and Skourup, C. (2010). Robot Automation in Oil and Gas Facilities: Indoor and Onsite Demonstrations. In *Proc. of IEEE/RSJ Int. Conf. on Intell. Rob. and Syst.*, 4729–4734.

Aspes, M., Bortoli, M., Orsenigo, L., and Maini, M. (1993). Multisensory Autonomous Robotic Inspection and Manipulation in an Unstructured Environment. *Conf. on Rem. Tech. for Nuclear Plant*, 63(3), 495–511.

Bengel, M., Pfeiffer, K., Graf, B., Bubeck, A., and Verl, A. (2009). Mobile Robots for Offshore Inspection and Manipulation. In *Proc. of IEEE/RSJ Int. Conf. on Intell. Rob. and Syst.*, 3317–3322.

Bouganis, C. and Brookes, M. (2004). Multiple Light Source Detection. *IEEE Trans. on Pattern Anal. and Mach. Intell.*, 26(4), 509–514.

Carvalho, G.P.S., Freitas, G.M., Costa, R.R., Carvalho, G.H.F., de Oliveira, J.F.L., Netto, S.L., da Silva, E.A.B., Xaud, M.F.S., Hsu, L., Motta-Ribeiro, G.C., Neves, A.F., Lizarralde, F., Marcovistz, I., Peixoto, A.J., Nunes, E.V.L., From, P.J., Galassi, M., and Røyrøy, A. (2013). DORIS - Monitoring Robot for Offshore Facilities. In *Proc. of Offshore Tech. Conf.*

Dellin, C., Strabala, K., Haynes, G.C., Stager, D., and Srinivasa, S. (2014). Guided Manipulation Planning at the DARPA Robotics Challenge Trials. In *Proc. of the Int. Symp. on Exp. Robot.*

From, P.J. (2010). *Off-Shore Robotics: Robust and Optimal Solutions for Autonomous Operation.* Ph.D. thesis, Norwegian University of Science and Technology.

Gao, X.S., Hou, X.R., Tang, J., and Cheng, H.F. (2003). Complete Solution Classification for the Perspective-three-point Problem. *IEEE Trans. on Pattern Anal. and Mach. Intell.*, 25(8), 930–943.

Guizzo, E. and Ackerman, E. (2012). How Rethink Robotics Built Its New Baxter Robot Worker. IEEE Spectrum.

Hebert, P., Bajracharya, M., Ma, J., Hudson, N., Aydemir, A., Reid, J., Bergh, C., Borders, J., Frost, M., Hagman, M., Leichty, J., Backes, P., and Kennedy, B. (2014). Mobile Manipulation and Mobility as Manipulation - Design and Algorithms of RoboSimian. *Jour. of Field Robot.*

Kyrkjebø, E., Liljebäck, P., and Transeth, A.A. (2009). A Robotic Concept for Remote Inspection and Maintenance on Oil Platforms. In *Proc. of ASME Int. Conf. on Ocean, Offshore and Arctic Engineering*, 667–674.

Lopez-Moreno, J., Garces, E., Hadap, S., Reinhard, E., and Gutierrez, D. (2013). Multiple Light Source Estimation in a Single Image. *Comp. Graph. Forum*, 32(8), 170–182.

NREC/CMU (2012). Sensabot: A Safe and Cost-Effective Inspection Solution. *Jour. of Petrol. Tech.*, 32–34.

Oberkampf, D., DeMenthon, D.F., and Davis, L.S. (1996). Iterative Pose Estimation Using Coplanar Feature Points. *Comp. Vis. Image Understand.*, 63(3), 495–511.

Palomeras, N., Ridao, P., Ribas, D., and Vallicrosa, G. (2014). Autonomous I-AUV Docking for Fixed-base Manipulation. In *Proc. of IFAC World Congress*, 12160–12165.

Quigley, M., Conley, K., Gerkey, B., Faust, J., Foote, T., Leibs, J., Wheeler, R., and Ng, A. (2009). ROS: An Open-source Robot Operating System. In *ICRA Workshop on Open Source Software*.

Siciliano, B., Sciavicco, L., Villani, L., and Oriolo, G. (2010). *Robotics: Modelling, Planning and Control.* Advanced Textbooks in Control and Signal Processing. Springer-Verlag London Ltd.

Trezona, P.W. (2001). Derivation of the 1964 CIE 10-degree XYZ Colour-Matching Functions and Their Applicability in Photometry. *Color Res. and App.*, 26(1), 67–75.

Trivedi, M., Chen, C., and Marapane, S. (1989). A Vision System for Robotic Inspection and Manipulation. *Computer*, 22(6), 91–97.

Yoon, W.K., Suehiro, T., Onda, H., and Kitagaki, K. (2005). Task Skill Transfer of Circle Handle Valve Manipulation. In *Proc. of IEEE Int. Wksp. on Rob. and Hum. Interact. Commun.*, 505–511.